Reaction Kinetics, Mechanisms and Catalysis (2022) 135:1703–1717
https://doi.org/10.1007/s11144-022-02214-w

Simple synthesis of high photocatalytic activity TiO_2 nanopowder with sodium dodecylbenzene sulfonate surfactant for photocatalysis of rhodamine B and methyl orange

Yu Wang[1] · Anze Shui[1] · Bin Du[2]

Received: 7 February 2022 / Accepted: 30 March 2022 / Published online: 7 April 2022

Abstract

In this study, the TiO_2 nanopowder with high photocatalytic activity has been successfully synthesized by a simple solvothermal method process without annealing by sodium dodecyl benzene sulfonate(SDBS) as surfactants. Meanwhile, effects of SDBS content on photocatalytic activity and properties of the TiO_2 nanopowder were systematically examined by the XRD, SEM, TEM, BET, XPS, UV–Vis DRS, TOC, photoelectrochemical and photodegradation experiments. The sample T without modification showed good photocatalytic performance under visible light irradiation. Its degradation efficiency of rhodamine B (RhB) and methyl orange (MO) was 3.6 times and 3.1 times that of P25, respectively. With the increase of the SDBS content, the photocatalytic activity of TiO_2 nanopowder was significantly improved. For degradation of RhB, the photocatalytic degradation efficiency of T-1.0wt%SDBS is 51 times that of P25. For degradation of MO, the photocatalytic degradation efficiency of T-1.0wt%SDBS is 5.3 times that of P25. And the related mechanisms were studied. These experimental results show that adding a small amount of SDBS in the simple synthesis process can observably enhance the specific surface area of TiO_2 and the amount of adsorbed O_2 and H_2O, thereby greatly improves the photocatalytic activity.

Keywords TiO_2 nanopowder · Surfactant · Visible light · Rhodamine B · Methyl orange

✉ Anze Shui
shuianze@scut.edu.cn

[1] School of Materials Science and Engineering, South China University of Technology, Guangzhou 510641, People's Republic of China

[2] School of Physics and Materials Science, Guangzhou University, Guangzhou 510006, People's Republic of China

Introduction

With the rapid development of the global economy and the continuous improvement in people's living standards, environmental pollution and energy crisis are becoming more and more serious. Global environmental governances and energy shortages are major challenges. In order to solve these problems, many researchers developed photocatalytic semiconductors. The achievement of semiconductor photocatalytic technology in the field of environmental remediation cannot be ignored [1, 2]. Photocatalytic semiconductors can be excited by sunlight to produce a series of redox reactions, which act an essential role in energy production and pollutant degradation. TiO_2 is considered to be the most ideal semiconductor for photocatalytic degradation because of its high stability, broad applicability and environment-friendly [3–9]. However, the photocatalytic degradation efficiency of TiO_2 under visible-light irradiation is far from satisfied to meet the requirement of practical application due to its wide bandgap and the fast recombination of photo-generated and electron–hole pairs.

Various methods have been exploited to improve the photocatalytic performance of TiO_2 over the past few years [10, 11]. Up to now, methods for improving the photocatalytic performance of TiO_2 mainly include changing the morphology, doping metal/nonmetal elements and combining with a second semiconductor to enhance the hole-electron separation capacity and visible light absorption. Esra Bilgin Simsek [12] successfully synthesized the boron doped TiO_2 by solvothermal method. Abbas Sadeghzadeh-Attar [13] synthesized aligned N–Fe codoped TiO_2 nanorods by a simple liquid-phase deposition process combined with a template-assisted approach. Liu et al. [14] combined WO_3 with GO/TiO_2 composite by sol–gel method. Kim et al. [15] used a two-phase thermal method to prepare two different topical TiO_2 nanocrystals, namely nanospheres and nanorods by adding two different surfactants, and better photocatalytic degradation efficiency was achieved when the nanospheres and nanorods mixed. But these methods cling to the infiltration of elements into TiO_2 lattices and the connection between the second phase and TiO_2 with complex process, and it is difficult to steadily control the photocatalytic performance. Moreover, the samples were annealed during the synthesis process, which increased the experimental cost.

According to the principle of photocatalysis, adsorption of pollutants and photocatalytic reaction mainly take place on the surface of catalysts [16, 17]. Therefore, the surface condition of photocatalyst is the most important factor to determine the adsorption capacity of pollutants and the photocatalytic reaction activity [18]. The molecular structure of surfactant changes the orientation and formation of micelles on the surface, which has good adsorption properties and can be used as dispersants in the synthesis of nanopowder. Many researchers have applied a variety of surfactants to the preparation and modification of photocatalyst, such as sodium dodecyl sulfate(SDBS) and hexadecyl trimethyl ammonium bromide(CTAB), and received lots of valuable results. Wu et al. [19] produced TiO_2 by sol–gel method, solvothermal method and annealing with hexadecyl trimethyl ammonium bromide(CTAB) as additives. Also TiO_2 with the addition of

CTAB had the largest surface area, with the photocatalytic degradation efficiency of MO improved. However, the photocatalytic degradation efficiency of TiO_2 was not too high. In addition, the processes were also complex to steadily control the photocatalytic performance. Therefore, a simple process to synthesize TiO_2 nanoparticle with high photocatalytic efficiency should be obtained.

In this study, a simple solvothermal method processed without annealing with sodium dodecyl benzene sulfonate (SDBS) as surfactants to synthesize TiO_2 nanopowder of high photocatalytic activity was reported, which could control steadily the photocatalytic performance. The effects of SDBS content on the surface area, bandgap, amount of oxygen vacancy and defect, electron–hole separation efficiency and photocatalytic performance of the TiO_2 nanopowder were examined in detail, and the related mechanisms were discussed.

Experimental

Photocatalyst preparation

First, 5.5 mL of tetrabutyl titanate(TBOT, from Enox) was mixed with 5.5 mL acetic acid(from Richjoint) and 31.5 mL 1-Propanol(from FUYU chemical reagent), denoted as A solution. Second, different contents of SDBS(DAMAO chemical reagent, 0 g, 0.05 g, 0.025 g and 0.01 g) were mixed with 37.5 mL deionized water and denoted as B1, B2, B3, B4, respectively. Then, A solution (39.6 ml) was slowly added into the B1, B2, B3 and B4 solution with vigorous stirring and stirred for 5 h, and then sonicated for 40 min in an ultrasonic bath. Finally, four groups of as-prepared mixture solution were transferred into a Teflon-lined stainless-steel autoclave at 150 °C for 9 h. The resultant precipitates were filtered and washed thoroughly with water and ethanol for several times and dried at 80 ℃ for 8 h under electronic oven. These samples were denoted as T, T-1.0wt%SDBS, T-0.5wt%SDBS and T-0.2wt%SDBS.

Material characterization

All the samples were analyzed by the X-ray diffractometer (XRD, XPert Pro, PANalytical B.V., the Netherlands) using Cu K_α radiation ($\lambda = 1.542$ Å), and the specific surface areas were measured by the Brunauer–Emmett–Teller (BET, Mike 2460) plots. As to the morphology and microstructures of the samples, they were characterized by scanning electron microscopy (SEM, SU8220, HITACHI, Japan) and Transmission electron microscopy (TEM, FEI, America), respectively. Generally, X-ray photoelectron spectroscopy (XPS) measurements were performed in a Thermo Scientific K-Alpha spectrometer to get chemical binding energy information of all samples. Meanwhile, the photoluminescence (PL) spectra of the samples were recorded with a PE LS 55 spectrofluorophotometer. The UV–Vis diffuse reflectance spectra (DRS) were determined by Lambda950.

Photodegradation experiment

Several quartz beakers with 200 mL volumes were utilized as reactors. Photodegradation efficiency was estimated by MO and RhB in an aqueous solution under visible light irradiation, with 300-W Xenon lamp (Changtu, China) possessing the 420 nm cutoff filter used as the irradiation source($\lambda > 425$ nm). Rhodamine B (RhB, $C_{28}H_{31}ClN_2O_3$) has a certain risk of carcinogenicity, and is generally used as a dye or a pollutant in photocatalytic experiments. Methyl orange (MO, $C_{14}H_{14}N_3SO_3Na$) has a certain carcinogenic risk, and is generally used as an acid–base indicator or a pollutant in photocatalytic experiments. In a series of photocatalytic degradation of RhB and MO experiment, 50 mg of the photocatalyst was dispersed in 50 mL of RhB (10 mg/L) and MO (10 mg/L) solution, respectively. The preparation method of dye solution is in the Supplementary Material (1). The suspension was stirred for 30 min in the dark to reach an adsorption–desorption equilibrium. The distance from the lamp to each sample was 12-14 cm. With the Xenon lamp turned on after the samples reached adsorption–desorption equilibrium, the suspension was taken at different time intervals for the degradation of RhB and MO. In order to remove the photocatalyst, four milliliters of suspension was collected and centrifuged. Then the residual RhB and MO concentrations were monitored by the UV–Vis spectrophotometer (UV1901PC), based on the maximum absorption at 554 nm and 464 nm. The total organic carbon (TOC) content of the solution in photocatalytic degradation was characterized by TOC analyzer (TOC-V, Japan).

Results and discussion

Characterizations of XRD, SEM, and TEM

In Fig. 1, the strong XRD peaks are observed at around 25.27°, 37.76°, 48.13°, 54.05°, 55.17° and 62.61°, which can be ascribed to (101), (004), (200), (105), (211) and (204) of anatase TiO_2(JCPDS card No. 21–1272), separately. In addition, no other peaks of the impurity can be observed in the XRD pattern, indicating the high purity of the as-obtained powders.

Fig. 2 shows the SEM images of the photocatalysts. It can be observed that the morphology of the T, T-1.0wt%SDBS, T-0.5wt%SDBS and T-0.2wt%SDBS are irregular. Obviously, the addition of SDBS for changing the morphology of TiO_2 is not effective. Since the precursor is a colloid, the TiO_2 samples of the experiment appear irregular. Therefore, the specific characteristics of the TiO_2 crystals need to be further explored.

The TEM images of the T and T-1.0wt%SDBS as is shown in Fig. 3. In order to create a more obvious contrast, T and T-1.0wt%SDBS were chosen to represent all SDBS-added samples. It can be observed that the lattice distances are 0.35 nm and 0.24 nm (Figs. 3b and d), corresponding to the (101) and (004) planes of the anatase phase respectively. Compared with the T sample, the electronic diffraction ring of T-1.0wt%SDBS is clearer and more coherent, which indicated that the crystalline character of T-1.0wt%SDBS is better. According to the Figs. 3a and c, it can be

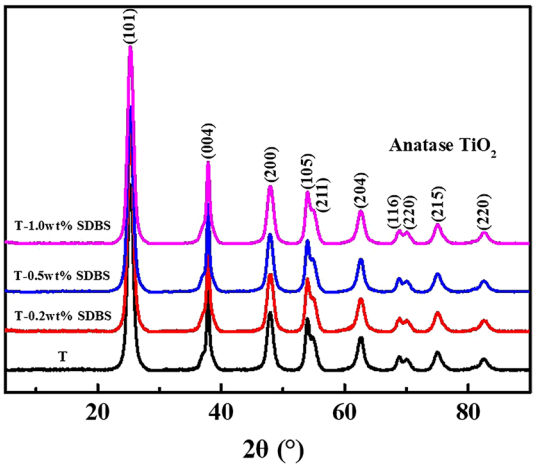

Fig. 1 XRD patterns of T, T-0.2wt%SDBS, T-0.5wt%SDBS and T-1.0wt%SDBS. (Condition: XPert Pro, PANalytical B.V., the Netherlands, Cu K_α 1.542 Å)

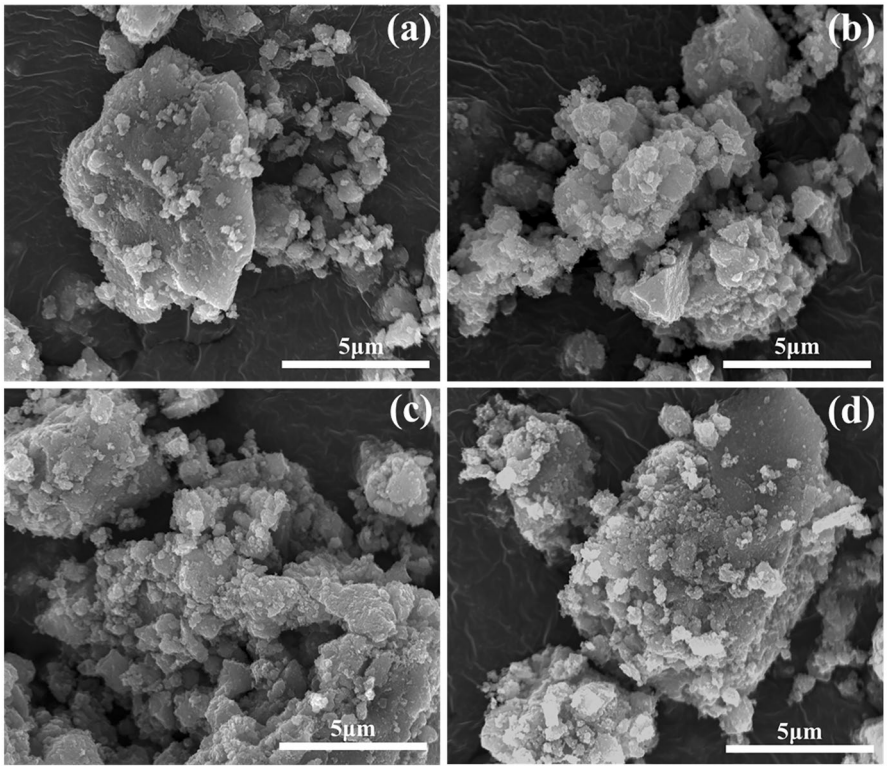

Fig. 2 SEM images of **a** T, **b** T-1.0wt%SDBS, **c** T-0.5wt%SDBS and **d** T-0.2wt%SDBS. (Condition: SU8220, HITACHI, Japan, HV 25 kV, WD 10 mm)

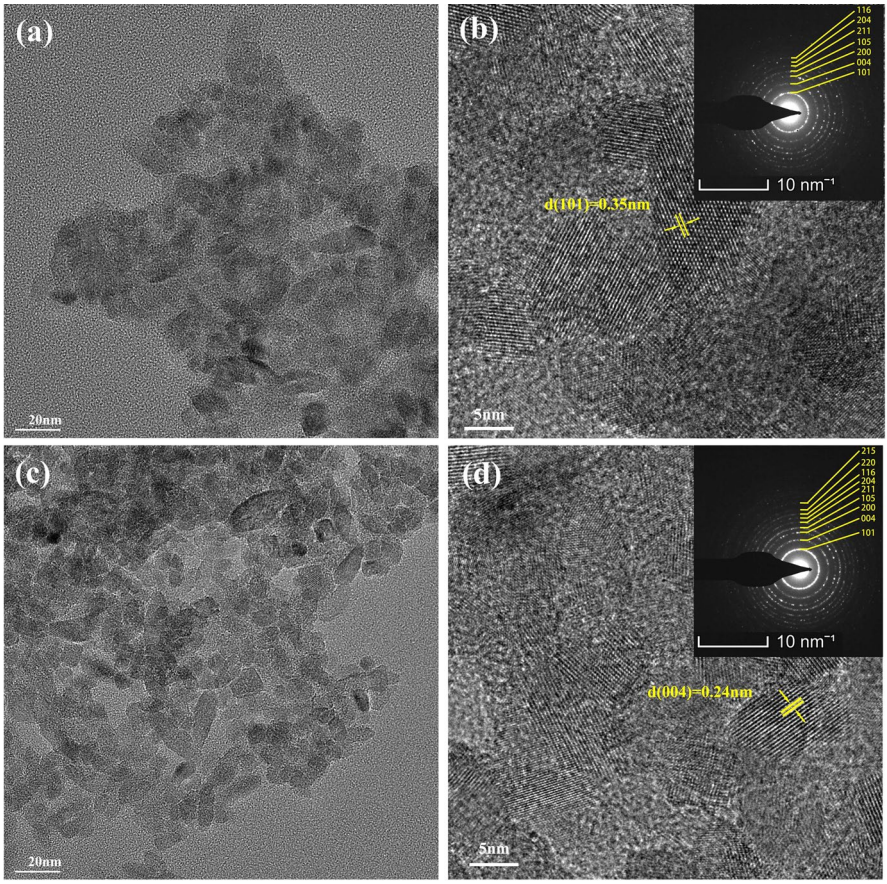

Fig. 3 TEM images of (**a**-**b**) T and (**c**-**d**) T-1.0wt%SDBS, Insets in the HR-TEM images show the selected-area electron diffraction pattern. (Condition: FEI, America)

easy to find that the distribution of grains of TiO_2 different from the lumps of SEM, with the grain size is between 5 and 20 nm. As an anionic surfactant, the existence of SDBS is conducive to the nucleation of TiO_2, hence, improving the crystallinity of TiO_2. Meanwhile, the surface energy of TiO_2 is higher than that of TiO_2 added SDBS and therefore, it is easier to agglomerate. After adding SDBS, the surface energy of TiO_2 particles decreases, it possesses outstanding dispersion performance [20]. These features also provide a prerequisite for improving the photocatalytic performance of SDBS-added samples.

Measurement of BET

Fig. S1a shows the N_2 adsorption–desorption isotherms and the pore size distribution plots of the T, T-1.0wt%SDBS and T-0.5wt%SDBS. The nitrogen adsorption–desorption isotherms of all samples show typical type IV isotherms, suggesting presents the

Table 1 Parameters of T, T-0.2wt%SDBS, T-0.5wt%SDBS and T-1.0wt%SDBS of BET

Sample	Surface area (m^2g^{-1})	Pore size (nm)	Pore volume (cm^3g^{-1})
T	165.6	6.26	0.24
T-0.5wt%SDBS	170.4	5.81	0.28
T-1.0wt%SDBS	175.4	6.01	0.30

Table 2 Parameters of Ti2p peaks and Curve-fitting results of the high resolution XPS spectra for the O1s region

Sample	TiO_2	T-0.2wt% SDBS	T-0.5wt% SDBS	T-1.0wt% SDBS
Ti 2p3/2(eV)	458.8	458.8	458.8	458.8
Ti 2p1/2(eV)	464.5	464.6	464.5	464.5
O_L	73.59%	71.08%	69.44%	68.59%
O_C	14.43%	16.63%	17.93%	19.29%
O_H	11.99%	12.29%	12.63%	12.12%

O_L: O1s core level peak at ca. 529.9 eV for TiO_2

O_C: O1s core level peak at ca. 530.4 eV for TiO_2

O_H: O1s core level peak at ca. 531.6 eV for TiO_2

mesoporous structures [21]. The shape of hysteresis loops was always used to identity the specific pore structures [22]. From Fig. S1a, the H2 hysteresis loops suggest the presence of pores with narrow necks and wide bodies(often referred to as 'ink bottle' pores) [22, 23]. Fig. S1b indicates the corresponding distribution plots of Barret-Joyner-Halenda (BJH) pore size, and Table 1 shows the related information of BET. It can be analyzed that pore sizes of all samples with SDBS added are concentrated in a smaller range. In addition, the surface area of T-0.5wt%SDBS and T-1.0wt%SDBS increased with the increase of SDBS content. The increase in specific surface area makes the contact of TiO_2 and degraded pollutants closer, and the electrons are easier to be trapped by oxygen vacancies and various defects which are conducive to the adsorption and photocatalytic degradation of degraded pollutants.

As a kind of anionic surfactant, SDBS can reduce the surface tension of solution and improve the dispersion of TiO_2 particles. In addition, the more uniformity pores TiO_2 has, the more uniform and regular hole channels samples possess [24]. Finally, compared with T, T-0.5wt%SDBS and T-1.0wt%SDBS have larger pore volumes, which may increase the adsorption of RhB and MO to a certain extent. The adsorption of degraded pollutants is often the first step in the process of photocatalytic degradation.

Measurement of XPS

Figs. S2 and S3 indicate the XPS survey spectra for the surface of TiO_2 with different content of SDBS, and relative parameter composition is listed in Table 2. Fig. S2a shows the XPS wide scan spectra of the samples. Obviously, all samples contain

Ti, O and C elements. No S element was detected, which proved that the S element of SDBS is not found to be doped into TiO_2, and the surfactant added during the synthesis process does not remain. The Ti2p spectrum is displayed in Fig. S2b, and the existence of TiO_2 was confirmed. The core level peak of Ti element didn't move after adding SDBS, which means that chemical states hadn't been changed. It can be seen from Table 1 and Fig. S2b that the peak difference between Ti2P3/2 peak and Ti2p1/2 peak was 5.7 eV ~ 5.8 eV [25], which confirmed the presence of Ti^{4+}.

High-resolution XPS spectra of the O1s region on the surfaces of the photocatalysts were illustrated with Fig. S3. The O1s can be fitted by their curves appearing at 529.8, 530.3, and 531.5 eV. The main peak belonging to the lattice oxygen atoms occurs at around 529.8 eV (labeled as O_L), chemisorbed O_2 at around 530.3 eV(labeled as O_C) and surface hydroxyl group at around 531.5 eV(labeled as O_H) [26]. The O_H that exists in four samples is attributable to the chemisorbed H_2O. Combining Fig. S3 and Table 2, it is concluded that the amount of O_C increases with the addition of sodium dodecyl benzene sulfonate. Some studies have shown that the photocatalytic degradation efficiency of TiO_2 is related to the adsorption of oxygen and surface hydroxyl groups. Generally, the existence of a certain amount of adsorbed oxygen and surface hydroxyl group might be a result of the increasing surface vacancies [23, 27, 28]. Therefore, the amount of oxygen vacancies in the TiO_2 sample with SDBS may be higher than that of the TiO_2 sample without SDBS. In photocatalytic reaction, oxygen vacancies can be applied as the active sites to combine with degraded pollutants, to promote the degradation of degraded pollutants. What's more,$\cdot O^{2-}$ and$\cdot$OH can be produced by chemisorbed O_2 and H_2O under visible-light irradiation [29], which are the main participants in the photocatalytic reaction. Therefore, the increase of O_H and O_C content on the surface of TiO_2 is conducive to the enhancement of photocatalytic activity [28].

Measurements of DRS and PL

In order to investigate the influence of SDBS content on the visible light absorption performance, UV–Vis diffuse reflectance spectra of T, T-0.5wt%SDBS, and T-1.0wt%SDBS were recorded by UV–Vis spectrophotometer. The bandgaps between all samples are estimated from plots of $(F(R)^* h\nu)^{1/2}$ versus $h\nu$, and the formula is:

$$(\alpha h\nu)^{1/2} = B\left(h\nu - E_g\right), \tag{1}$$

Here h, ν, B, E_g,α denote respectively the Planck constant, frequency of light, a physical quantity related to the material, band gap energy, absorbance.

The Kubelka–Munk formula is:

$$F(R) = (1 - R)(1 - R)/2R, \tag{2}$$

Here R is the reflectivity.

The results are shown in Fig. S4b. With the increase of SDBS content, absorption edges are slightly red-shifted (shown in Fig. S4a). According to the Fig. S4b, it can

be concluded that the band gaps decrease slightly with the increase of SDBS content, which are 3.03 eV, 3.02 eV, 3.0 eV and 2.97 eV. However, this change is quite slight, which can be considered as the result of adding SDBS, which did not significantly change the band gap of TiO_2. In addition, the band gaps of all samples are less than the standard band gap (3.2 eV) of P25, which may be helpful to improve the photocatalytic degradation efficiency. Therefore, the photocatalytic degradation efficiency of the samples in this experiment may be significantly higher than that of P25.

Fig. S5 shows the PL spectra of the four samples with the excitation wavelength of 220 nm. It can be found that all samples could exhibit obvious PL signals with similar curve shapes. With the content of SDBS increasing, the PL signal is gradually enhanced. When the energy of the radiative photon is lower than the bandgap energy, and the emission wavelength of the radiative photon is longer than the wavelength of bandgap energy, hence, the PL signal is attributed to a kind of excitonic PL process [30]. In general, the excitonic PL signal mainly results from surface oxygen vacancies and defects of semiconductors. The excitonic PL intensity rises up with the increase of surface oxygen vacancy and defect content, which means the adding of SDBS during the synthesis process causes more oxygen vacancies and defects on the surface of the samples. Therefore, the amount of surface oxygen vacancy and defect increase with the existence of more SDBS, which is consistent with the analysis results of XPS. The surface oxygen vacancy and defect can trap electrons easily [31], which is beneficial to increase electron–hole separation efficiency and ability of photodegradation.

Evaluation and analysis photocatalytic activity

The photocatalytic activity of the photocatalyst was carried out through the removal of RhB and MO with equal time variation under visible light [32]. In addition, the P25(a commercial TiO_2 photocatalyst) was also used to evaluate the photocatalytic properties of this work. The adsorption–desorption equilibrium of TiO_2 is usually in 30 min. In order to define the adsorption–desorption equilibrium of all simples during a dark reaction, we made an experiment. Fig. S6 shows the adsorption–desorption process of samples in dark reaction, which can prove that the sample achieves the adsorption–desorption equilibrium within 30 min.

The photocatalytic degradation processes of the T, T-0.2wt%SDBS, T-0.5wt%SDBS and T-1.0wt%SDBS can be seen in Fig. S7 and S8. Fig. S7a and S8a show the photocatalytic degradation curves of RhB and MO, respectively. It could be found that all samples have better photocatalytic degradation ability than the P25, And the photocatalytic activity of the samples synthesized by adding SDBS is higher than that of the sample T [33]. Notably, T-1.0wt%SDBS exhibits the highest photocatalytic activity, indicating that with increasing SDBS content, the photocatalytic efficiency is significantly improved.

Application of non-linear least squares fitting to our experimental data was performed by using Excel file kindly provided by Prof. Gábor Lente at http://lenteg.ttk.pte.hu/KinetFit.html. The results are shown in Figs. S7b and S8b, and the

Table 3 Kinetic parameters of photocatalytic degradation of RhB obtained by nonlinear least squares fitting

RhB	K (min^{-1})	Standard errors	X	Standard errors	E	Standard errors	R2
T	0.1162	0.0160	1.020	0.0448	0.1095	0.0284	0.9933
T-0.2wt%SDBS	0.2962	0.0127	0.8505	0.0159	−0.0608	0.0172	0.9966
T-0.5wt%SDBS	0.7068	0.0126	0.6851	0.0047	−0.0164	0.0032	0.9984
T-1.0wt%SDBS	1.646	0.0153	0.5150	0.0015	0.0060	0.0007	0.9997
P25	0.0323	0.0069	1.4785	0.0774	0.3141	0.0178	0.9988

Table 4 Kinetic parameters of photocatalytic degradation of MO obtained by nonlinear least squares fitting

MO	K (min^{-1})	Standard errors	X	Standard errors	E	Standard errors	R2
T	0.0459	0.0065	0.6844	0.0427	0.1831	0.0447	0.9837
T-0.2wt%SDBS	0.0519	0.0032	0.8034	0.0205	0.0837	0.0211	0.9963
T-0.5wt%SDBS	0.0680	0.0006	0.9229	0.0068	−0.0921	0.0072	0.9999
T-1.0wt%SDBS	0.0781	0.0016	0.9190	0.0142	−0.1117	0.0149	0.9990
P25	0.0147	0.0107	0.5227	0.0117	0.9818	0.0154	0.9571

relevant data can be found in Tables 3 and 4. According to Figs. S7b and S8b, the RhB photodegradation rate constant(k) values of T-1.0wt%SDBS, T-0.5wt%SDBS, T-0.2wt%SDBS, T and P25 are determined to be 1.646, 0.7068, 0.2962, 0.1162 and 0.0323 min^{-1}, respectively. The MO photodegradation rate constant(k) values of T-1.0wt%SDBS, T-0.5wt%SDBS, T-0.2wt%SDBS, T and P25 are determined to be 0.078, 0.068, 0.0519, 0.0459 and 0.0147 min^{-1}. For degradation of RhB, the photocatalytic degradation efficiency of T-1.0wt%SDBS is 51 times that of P25 and 14 times that of T. For degradation of MO, the photocatalytic degradation efficiency of T-1.0wt%SDBS is 5.3 times that of P25 and 1.7 times that of T. These results show that the addition of SDBS significantly improves the photocatalytic activity of the samples, which is significant in the current research progress to improve the efficiency of TiO_2 photocatalytic degradation.

Due to the large adsorption capacity of the reactants, the reproducibility of photocatalytic degradation is quite important. The sample T-0.5wt%SDBS was used as an example to explore the reproducibility of photocatalytic reactions. The stability and reusability of TiO_2 nanoparticles were further investigated. Fig. S9 shows the 5-cycle test for RhB and MO degradation by T-0.5wt%SDBS under visible-light irradiation. The loss of TiO_2 nanoparticles was below 10% during washing and reusing. It can be seen that the T-0.5wt%SDBS sample previously prepared has good recyclability, which proves that the degraded pollutants adsorbed on the surface by TiO_2 during the dark reaction can be degraded under visible-light irradiation. Photos of T-0.5wt%SDBS and solution in photocatalytic experiment were shown in Fig. S10. The centrifuge tubes from right to left in the picture are the white sample T-0.5wt%SDBS before photocatalysis, T-0.5wt%SDBS after adsorption and T-0.5wt%SDBS after photocatalysis. In fact, the color of the prepared white samples

changed after the dark reaction for 30 min: for one thing, the color changed into light pink when adsorbed RhB. For another, the color changed into light yellow when adsorbed MO, which reached the adsorption–desorption equilibrium. After the photocatalytic degradation reaction, the color of samples turned white again. Combining Fig. S7 and S8, it can be inferred that the adsorption of degraded pollutants is the first step of photocatalytic degradation. Improving the ability of samples to adsorb degraded pollutants may improve the efficiency of photocatalytic degradation under visible-light irradiation. Table 5 compares our results with previous works [34–36].

To further investigate the photocatalytic degradation of RhB and MO by our samples, we tested the mineralization of RhB and MO in the photocatalytic process. In order to make the comparison more obvious, we chose the photocatalytic process of T-1.0wt%SDBS and P25 for the TOC test. To compare with the previous photocatalytic results, the TOC test results are presented in the form of TOC/TOC_0, which corresponds to Fig. S11. The TOC concentrations of the initial RhB and MO solutions were 11.25 mg/L and 8.36 mg/L, respectively. From Fig. S11, we can see that the content of TOC decreases with the extension of light irradiation time, which proves parts of RhB and MO are degraded. However, different from the photocatalytic degradation rate, 27.8%TOC remained in RhB solution after 6 min of light irradiation in the photocatalytic process of T-1.0wt%SDBS, and 38.2%TOC remained in MO solution after 40 min of light irradiation. Our analysis are as follows. First, the TOC contents in the initial RhB and MO solutions are 11.25 mg/L and 8.36 mg/L, while the theoretical values should be 7.2 mg/L and 5.2 mg/L. The extra part may be organic impurities and measurement errors in water, so the value of TOC/TOC_0 is always larger than C/C_0. In addition, RhB and MO were not completely degraded into CO_2 and H_2O in the photocatalytic reaction but generated short chain organics [37, 38], which slowed down the decrease of organic carbon content in the solution.

Based on the above experiments, we propose the photocatalytic reaction mechanism of RhB and MO under visible light. We take the T-0.5wt%SDBS as an example. As shown in Fig. S12, under the irradiation of visible light, the T-0.5wt%SDBS can be excited and generate electron and hole pairs. Subsequently, the electrons migrated to CB can react with O_2 to generate $\cdot O_2^-$, and part of the holes left in VB can react with OH^- of H_2O to generate ·OH. The $\cdot O_2^-$, ·OH and h^+ can react with dyes to complete photodegradation.

According to the previous characterization, the improvement of photocatalytic degradation efficiency of TiO_2 can be explained as follows. First, with increasing

Table 5 Comparison of our results with the literatures

Photocatalyst	RhB%	Initial concentrationand	MO%	Initial concentration	References
TiO_2	98.94%(3 min)	10 mg/L(50 ml)	95.73%(40 min)	10 mg/L(50 ml)	Ours
SnS_2	93.67%(3 h)	10 mg/L(50 ml)	×	×	[36]
Cu_2O	43%	10 mg/L(100 ml)	82%	10 mg/L(100 ml)	[35]
ZnO	62%	10 mg/L(100 ml)	53%	10 mg/L(100 ml)	[35]
ZnO/Bentonite	92%	5 mg/L	×	×	[34]

of SDBS content, the content of oxygen vacancy and defect in TiO_2 also increases, which is beneficial to trap the transition electrons, reduce the possibility of electron hole recombination and improve the separation efficiency of electron and hole. At the same time, the amount of O_2 and H_2O adsorbed by TiO_2 also increases. In the photocatalytic reaction, $\cdot O_2^-$ and ·OH are produced by chemisorbed O_2 and H_2O under visible-light irradiation, which are the main participants in the photocatalytic reaction. Second, the surface area of TiO_2 nanoparticles increases with the augment of SDBS content and leads to providing more active sites for redox reactions. When the TiO_2 nanoparticles size decreases, the free path of electrons also decreases, then the electrons are easier to be trapped by oxygen vacancies and various defects. Meanwhile, the photocatalytic efficiency increases with the increase of SDBS content, but the adsorption capacity also increases during the 30-min dark adsorption reaction. The specific surface area and pore volume enhance with the SDBS contents, therefore, T-1.0wt%SDBS has the most excellent adsorption performance. The adsorption of degraded pollutants on the surface of TiO_2 may be the first step in the photocatalytic degradation reaction. Therefore, samples that can adsorb more degraded pollutants may have higher photocatalytic degradation efficiency.

However, excellent adsorption performances also have an effect on the calculation of the photocatalytic degradation rate, and the adsorption capacity of the T-1.0wt%SDBS for RhB is close to 50%, so continuing to improve the ratio of SDBS is unnecessary. The adsorption capacity of our samples is too large, so the reduction of adsorption rate while further improving photocatalytic degradation efficiency remains to be solved.

Conclusion

TiO_2 nanopowder with high photocatalytic activity under visible-light irradiation was prepared by a simple solvothermal method process without annealing with TBOT as raw material and SDBS as surfactant at 150 °C. The effects of SDBS content on photocatalytic activity and properties of TiO_2 nanopowder were systematically examined, and the related mechanisms were discussed. Compared with the commercial P25, the photocatalytic degradation efficiency of TiO_2 nanopowder with 1.0 wt%SDBS was greatly improved. For degradation of RhB, the photocatalytic degradation efficiency of T-1.0wt%SDBS is 51 times that of P25 and 14 times that of T. For degradation of MO, the photocatalytic degradation efficiency of T-1.0wt%SDBS is 5.3 times that of P25 and 1.7 times that of T, which proves the importance of SDBS to enhance the performance of TiO_2.

The excellent photocatalytic efficiency can be attributed to the following reasons. First, with increasing SDBS content, the amount of oxygen vacancy and defect in TiO_2 increase, which can trap the transition electrons and improve the separation efficiency of electron and hole. Meanwhile, the amount of O_2 and H_2O adsorbed by the TiO_2 also increases, which can produce $\cdot O_2^-$ and ·OH and improve photocatalytic degradation efficiency. Second, the surface area enhances with increasing SDBS content, which provides more active sites for redox reactions, and simultaneously improves the adsorption capacity of TiO_2.

Supplementary Information The online version contains supplementary material available at https://doi.org/10.1007/s11144-022-02214-w.

Acknowledgements This work was supported by the National Natural Science Foundation of China (51972114, 51772102, 52102065), National Natural Science Foundation of Guangdong Province (2019A1515011992), Guangdong YangFan Innovative & Entrepreneurial Research Team Program (2016YT03C327) and Zhujiang Delta Water Resources Allocation Project (CD88-GC02-2020-0012).

Declarations

Conflict of interest On behalf of all authors, the corresponding author states that there is no conflict of interest.

References

1. Cao S, Liu T, Tsang Y, Chen C (2016) Role of hydroxylation modification on the structure and property of reduced graphene oxide/TiO_2 hybrids. Appl Surf Sci 382:225–238. https://doi.org/10.1016/j.apsusc.2016.04.138
2. Kumar SG, Rao KSRK (2017) Comparison of modification strategies towards enhanced charge carrier separation and photocatalytic degradation activity of metal oxide semiconductors (TiO_2, WO_3 and ZnO). Appl Surf Sci 391:124–148. https://doi.org/10.1016/j.apsusc.2016.07.081
3. She H, Ma X, Chen K, Liu H, Huang J, Wang L, Wang Q (2020) Photocatalytic H_2 production activity of TiO_2 modified by inexpensive $Cu(OH)_2$ cocatalyst. J Alloy Compd. https://doi.org/10.1016/j.jallcom.2019.153239
4. Xu T, Zhao H, Zheng H, Zhang P (2020) Atomically Pt implanted nanoporous TiO_2 film for photocatalytic degradation of trace organic pollutants in water. Chem Eng J. https://doi.org/10.1016/j.cej.2019.123832
5. Natarajan S, Bajaj HC, Tayade RJ (2018) Recent advances based on the synergetic effect of adsorption for removal of dyes from waste water using photocatalytic process. J Environ Sci (China) 65:201–222. https://doi.org/10.1016/j.jes.2017.03.011
6. Nakata K, Ochiai T, Murakami T, Fujishima A (2012) Photoenergy conversion with TiO_2 photocatalysis: New materials and recent applications. Electrochim Acta 84:103–111. https://doi.org/10.1016/j.electacta.2012.03.035
7. Liu K, Cao M, Fujishima A, Jiang L (2014) Bio-inspired titanium dioxide materials with special wettability and their applications. Chem Rev 114:10044–10094. https://doi.org/10.1021/cr4006796
8. Bessekhouad Y, Robert D, Weber JV (2003) Synthesis of photocatalytic TiO_2 nanoparticles: optimization of the preparation conditions. J Photochem Photobiol, A 157:47–53. https://doi.org/10.1016/s1010-6030(03)00077-7
9. Einaga H, Takashi I, Shigeru F (2004) Improvement of catalyst durability by deposition of Rh on TiO_2 in photooxidation of aromatic compounds. Environ Sci Technol 38:285–289. https://doi.org/10.1021/es034336v
10. Dinh CT, Yen H, Kleitz F, Do TO (2014) Three-dimensional ordered assembly of thin-shell Au/TiO_2 hollow nanospheres for enhanced visible-light-driven photocatalysis. Angew Chem Int Ed Engl 53:6618–6623. https://doi.org/10.1002/anie.201400966
11. Li Z, Gao B, Chen GZ, Mokaya R, Sotiropoulos S, Li Puma G (2011) Carbon nanotube/titanium dioxide (CNT/TiO_2) core–shell nanocomposites with tailored shell thickness, CNT content and photocatalytic/photoelectrocatalytic properties. Appl Catal B 110:50–57. https://doi.org/10.1016/j.apcatb.2011.08.023
12. Bilgin Simsek E (2017) Solvothermal synthesized boron doped TiO_2 catalysts: Photocatalytic degradation of endocrine disrupting compounds and pharmaceuticals under visible light irradiation. Appl Catal B 200:309–322. https://doi.org/10.1016/j.apcatb.2016.07.016
13. Sadeghzadeh-Attar A (2019) Photocatalytic degradation evaluation of N-Fe codoped aligned TiO2 nanorods based on the effect of annealing temperature. J Adv Ceramic. https://doi.org/10.1007/s40145-019-0353-1

14. Liu X, Chen C, X.a. Chen, G. Qian, J. Wang, C. Wang, Z. Cao, Q. Liu, (2018) WO_3 QDs enhanced photocatalytic and electrochemical perfomance of GO/TiO_2 composite. Catal Today 315:155–161. https://doi.org/10.1016/j.cattod.2018.02.037
15. Kim JY, Choi SB, Kim DW, Lee S, Jung HS, Lee J-K, Hong KS (2008) Surfactant-assisted shape evolution of thermally synthesized TiO_2 nanocrystals and their applications to efficient photoelectrodes. Langmuir 24:4316–4319. https://doi.org/10.1021/la703497e
16. Hoffmann MR, Martin ST, Choi W, Bahnemann DW (1995) Environmental applications of semiconductor photocatalysis. Chem Rev 95:69–96. https://doi.org/10.1021/cr00033a004
17. Chen X, Mao SS (2007) Titanium dioxide nanomaterials synthesis, properties, modifications, and applications. Chem Rev 107:2891–2959. https://doi.org/10.1021/cr0500535
18. Farghali AA, Zaki AH, Khedr MH (2016) Control of Selectivity in Heterogeneous Photocatalysis by Tuning TiO_2 Morphology for Water Treatment Applications. Nanomaterials and Nanotechnology. https://doi.org/10.5772/62296
19. Wu W, Zhang L, Zhai X, Liang C, Yu K (2018) Preparation and photocatalytic activity analysis of nanometer TiO_2 modified by surfactant. Nanomaterials and Nanotechnology. https://doi.org/10.1177/1847980418781973
20. Zhang C, Chen R, Zhou J, Cheng J, Xia Q (2009) Synthesis of TiO_2 films on glass slides by the sol-gel method and their photocatalytic activity. Rare Met 28:378–384. https://doi.org/10.1007/s12598-009-0075-6
21. Cho KM, Kim KH, Choi HO, Jung H-T (2015) A highly photoactive, visible-light-driven graphene/2D mesoporous TiO_2 photocatalyst. Green Chem 17:3972–3978. https://doi.org/10.1039/c5gc00641d
22. Sing KSW (1985) Reporting physisorption data for gas/solid systems with special reference to the determination of surface area and porosity. Pure Appl Chem 57:603–619. https://doi.org/10.1351/pac198557040603
23. Jing L, Xu Z, Sun X, Shang J, Cai W (2001) The surface properties and photocatalytic activities of ZnO ultrafine particles. Appl Surf Sci 180:308–314. https://doi.org/10.1016/S0169-4332(01)00365-8
24. Hu M, Cao Y, Li Z, Yang S, Xing Z (2017) Ti^{3+} self-doped mesoporous black TiO_2 /SiO_2 nanocomposite as remarkable visible light photocatalyst. Appl Surf Sci 426:734–744. https://doi.org/10.1016/j.apsusc.2017.07.178
25. Yu J, Pang Z, Zheng C, Zhou T, Zhang J, Zhou H, Wei Q (2019) Cotton fabric finished by PANI/TiO_2 with multifunctions of conductivity, anti-ultraviolet and photocatalysis activity. Appl Surf Sci 470:84–90. https://doi.org/10.1016/j.apsusc.2018.11.112
26. Zeng L, Song W, Li M, Zeng D, Xie C (2014) Catalytic oxidation of formaldehyde on surface of $HTiO_2$/$HCTiO_2$ without light illumination at room temperature. Appl Catal B 147:490–498. https://doi.org/10.1016/j.apcatb.2013.09.013
27. Wu JM, Tang ML (2011) One-pot synthesis of N-F-Cr-doped anatase TiO_2 microspheres with nearly all-(001) surface for enhanced solar absorption. Nanoscale 3:3915–3922. https://doi.org/10.1039/c1nr10737b
28. Yu JC, Yu J, Zhao J (2002) Enhanced photocatalytic activity of mesoporous and ordinary TiO_2 thin films by sulfuric acid treatment. Appl Catal B 36:31–43. https://doi.org/10.1016/S0926-3373(01)00277-6
29. Yang W, Chen Y, Gao S, Sang L, Tao R, Sun C, Shang JK, Li Q (2021) Post-illumination activity of Bi2WO6 in the dark from the photocatalytic "memory" effect. Journal of Advanced Ceramics 10:355–367. https://doi.org/10.1007/s40145-020-0448-8
30. Liqiang J, Yichun Q, Baiqi W, Shudan L, Baojiang J, Libin Y, Wei F, Honggang F, Jiazhong S (2006) Review of photoluminescence performance of nano-sized semiconductor materials and its relationships with photocatalytic activity. Sol Energy Mater Sol Cells 90:1773–1787. https://doi.org/10.1016/j.solmat.2005.11.007
31. Liqiang J, Xiaojun S, Baifu X, Baiqi W, Weimin C, Honggang F (2004) The preparation and characterization of La doped TiO_2 nanoparticles and their photocatalytic activity. J Solid State Chem 177:3375–3382. https://doi.org/10.1016/j.jssc.2004.05.064
32. Zhang G, Sun Z, Hu X, Song A, Zheng S (2017) Synthesis of BiOCl/TiO_2 –zeolite composite with enhanced visible light photoactivity. J Taiwan Inst Chem Eng 81:435–444. https://doi.org/10.1016/j.jtice.2017.09.030

33. Si Y, h. Liu, N. Li, J. Zhong, J. Li, D. Ma, (2018) SDBS-assisted hydrothermal treatment of TiO2 with improved photocatalytic activity. Mater Lett 212:147–150. https://doi.org/10.1016/j.matlet.2017.10.088
34. Boutra B, Trari M (2017) Solar photodegradation of a textile azo dye using synthesized ZnO/Bentonite. Water Sci Technol 75:1211–1220. https://doi.org/10.2166/wst.2016.597
35. Boughelout A, Macaluso R, Kechouane M, Trari M (2020) Photocatalysis of rhodamine B and methyl orange degradation under solar light on ZnO and Cu2O thin films. React Kinet Mech Catal 129:1115–1130. https://doi.org/10.1007/s11144-020-01741-8
36. Kabouche S, Louafi Y, Bardeau JF, Trari M (2018) Synthesis, physical and semiconducting properties of SnS2 prepared by chemical route. J Mater Sci: Mater Electron 30:687–694. https://doi.org/10.1007/s10854-018-0337-x
37. Soltani T, Entezari MH (2013) Sono-synthesis of bismuth ferrite nanoparticles with high photocatalytic activity in degradation of Rhodamine B under solar light irradiation. Chem Eng J 223:145–154. https://doi.org/10.1016/j.cej.2013.02.124
38. Yu X, Kou S, Nie J, Zhang J, Wei Y, Niu J, Yao B (2018) Preparation and performance of Cu2O/TiO2 nanocomposite thin film and photocatalytic degradation of Rhodamine B. Water Sci Technol 78:913–924. https://doi.org/10.2166/wst.2018.369